



## Article

# Synthesis and Characterization of Supercapacitor Materials from Soy

Iris Denmark <sup>1</sup>, Amna Khan <sup>2</sup>, Taylor Scifres <sup>1</sup>, Tito Viswanathan <sup>1</sup>, Fumiya Watanabe <sup>3</sup> and Noureen Siraj <sup>1,\*</sup>

<sup>1</sup> Department of Chemistry, University of Arkansas at Little Rock, 2801 S. University Ave, Little Rock, AR 72204, USA; isdenmark@ualr.edu (I.D.); tbscifres@ualr.edu (T.S.); txviswanatha@ualr.edu (T.V.)

<sup>2</sup> Little Rock Central High School, Little Rock, AR 72202, USA; akaykhan@gmail.com

<sup>3</sup> Center for Integrative Nanotechnology Sciences, University of Arkansas at Little Rock, 2801 S. University Ave, Little Rock, AR 72204, USA; fxwatanabe@ualr.edu

\* Correspondence: nxsiraj@ualr.edu

**Abstract:** Renewable resources and their byproducts are becoming of growing interest for alternative energy. Here, we have demonstrated the use of Arkansas' most important crop, soy, as a carbon precursor for the synthesis of carbonized activated materials for supercapacitor applications. Different soy products (soymeal, defatted soymeal, soy flour and soy protein isolate) were converted into carbonized carbon and co-doped with phosphorus and nitrogen simultaneously, using a facile and time-effective microwave synthesis method. Ammonium polyphosphate was used as a doping agent which also absorbs microwave radiation. The surface morphology of the resulting carbonized materials was characterized in detail using scanning electron microscopy. X-ray photoelectron spectroscopy was also performed, which revealed the presence of a heteroelemental composition, along with different functional groups at the surface of the carbonized materials. Raman spectroscopy results depicted the presence of both a graphitic and defect carbon peak, with defect ratios of over one. The electrochemical performance of the materials was recorded using cyclic voltammetry in various electrolytes including acids, bases and salts. Among all the other materials, soymeal exhibited the highest specific capacitance value of 127 F/g in acidic electrolytes. These economic materials can be further tuned by changing the doping elements and their mole ratios to attain exceptional surface characteristics with improved specific capacitance values, in order to boost the economy of Arkansas, USA.

**Keywords:** soy; co-doped carbon; electrical double layer capacitor; cyclic voltammetry; electrolyte ionic size



**Citation:** Denmark, I.; Khan, A.; Scifres, T.; Viswanathan, T.; Watanabe, F.; Siraj, N. Synthesis and Characterization of Supercapacitor Materials from Soy. *Electrochem* **2021**, *2*, 534–545. <https://doi.org/10.3390/electrochem2040034>

Academic Editor: Masato Sone

Received: 3 September 2021

Accepted: 11 October 2021

Published: 14 October 2021

**Publisher's Note:** MDPI stays neutral with regard to jurisdictional claims in published maps and institutional affiliations.



**Copyright:** © 2021 by the authors. Licensee MDPI, Basel, Switzerland. This article is an open access article distributed under the terms and conditions of the Creative Commons Attribution (CC BY) license (<https://creativecommons.org/licenses/by/4.0/>).

## 1. Introduction

The current global economy is substantially driven by energy produced by fossil fuels, which are non-renewable resources derived from animal and plant remains formed millions of years ago [1–3]. Though these resources have become easily acquirable and convenient to utilize in the modern age, fossil fuel resources have depleted throughout the years. Moreover, the burning of fossil fuels to acquire energy releases toxins into the environment which has been shown to negatively impact our climate. With the increasing demand for fossil fuels, speculation regarding the consistent depletion of fossil fuels and the addressing of environment pollution, the pathway to innovations of alternative energy sources has recently broadened.

Recently, supercapacitors have been getting tremendous attention for addressing potential energy crises in the future. Supercapacitors are portable sources of alternative energy that operate under low voltages and have very high charge/discharge rates [4,5]. Current applications of supercapacitors can be seen in various industries such as automobiles and small devices [6,7]. They are optimal because they have the capability to

store energy both electrostatically via electrochemical double layer (EDL) formation, as well as electrochemically via redox reactions of electrolyte ions adsorbed onto the surface of the active supercapacitor material [8,9]. Today's commercial supercapacitors utilize expensive active materials made from metals and metal oxides that show dull cycling stability [10] and require timely synthesis protocols [11–15]. Thus, it is imperative to find more economical materials that can be easily utilized as supercapacitor materials.

Carbon is one of the most abundant elements in nature. It is inexpensive, bioavailable and environmentally friendly. Many researchers have investigated different carbon-based materials derived from renewable resources such as thiamine [16], tannin [17–19], used tea [20,21], coffee grounds [22–24], cornstalk [25,26], molasses [27,28], bamboo leaves [29], cotton [30] and many more for supercapacitor applications. Similarly, soy has also been demonstrated as being effective in charge storage applications by Huo et al. [31] and Herde et al. [32], yielding specific capacitance values as low as 4 F/g, and as high as 115 F/g. The soybean is a very prominent source of carbon, and is also one of Arkansas' most important crops, ranking 11th in the nation for soybean production as of 2019 statistics reported by the University of Arkansas [33]. Therefore, any increase in specific capacitance of soy material is highly desirable. Traditionally, carbon materials are doped with heteroatoms to enhance their conductive properties and charge storage characteristics using functional groups at the surface of the materials. Doped carbon materials have been utilized in many applications ranging from sensors [34], bioimaging [35] and for use in alternative energy sources such as fuel cells [36] and supercapacitors [19,27,37]. In this work, renewable resources (soy products) are used to produce doped carbon materials for supercapacitor applications using a green and time-efficient microwave synthesis protocol.

One pertinent factor in the performance of carbon-based supercapacitors are the interfacial reactions that occur between supercapacitor materials and the electrolyte. An electrolyte is a solution of free-flowing ions which plays a significant role in the electrochemical performance of supercapacitors. Many electrolyte features such as ion size [38,39], thermal stability [40] and potential windows [41,42] greatly affect overall performance of supercapacitor materials, especially that of porous carbon materials to which pore-size is a primary determinant of electrolyte performance. Aqueous electrolytes commonly used are acids and bases. However, salt solutions may also be used as electrolytes for the electrochemical assessment of supercapacitors. They are neutral, very low in environmental toxicity and are cost-efficient. However, the size of ions in the salts significantly affects the performance of the supercapacitor material. Therefore, the roles of cation and anion are studied here in detail. Salt electrolytes offer thermal stability and allow for consistent electrochemical behavior.

Here, a series of phosphorus and nitrogen co-doped carbon materials were synthesized from soy-based carbon precursors. Simple and inexpensive microwave equipment was used to prepare doped carbonized carbon. Four different soy sources i.e., soy flour, soymeal, defatted soymeal and soy protein isolate were used. All of these materials are characterized physically using scanning electron microscopy, X-ray photoelectron spectroscopy and Raman spectroscopy. In electrochemical studies, the most commonly acidic and basic aqueous electrolytes, as well as salts of two different cation and anions, are used to investigate the role of ionic size in salts on supercapacitor performance. For the first time, doped carbon materials derived from soy-based renewable sources from a facile microwave method are prepared and explored for energy storage applications.

## 2. Experimental

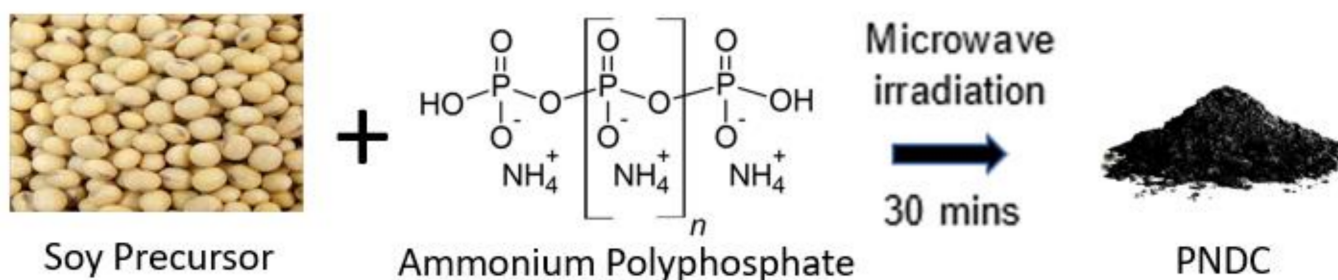
### 2.1. Materials

Soymeal (Assi brand, Gyeonggi-do, Korea) was purchased from a local grocery store in Little Rock, Ar. The hexane-processed soymeal and defatted soy flour was gifted from the department of agriculture at the University of Arkansas at Little Rock. Soy protein isolate (Profam 825) was received from ADM (Decatur, IL, USA). Ammonium polyphosphate (APP) ( $MW = 97 \text{ g mol}^{-1}$ ) was gifted from CheMarCo Inc. (Greenville, SC, USA). Potassium

chloride (KCl) was purchased from Spectrum Chemical (Gardena, CA, USA). Potassium hydroxide (KOH), potassium nitrate (KNO<sub>3</sub>), sodium nitrate (NaNO<sub>3</sub>), sodium chloride (NaCl) sulfuric acid (H<sub>2</sub>SO<sub>4</sub>), and 99% ethanol were purchased from Sigma-Aldrich (St. Louis, MO, USA). Carbon black was obtained from Cabot Chemical (Boston, MA, USA). The 5% Nafion D-520 was purchased from Bean Town Chemical (Hudson, NH, USA).

## 2.2. Co-Doping of Soy Materials with Phosphorus and Nitrogen

Soy materials were co-doped with phosphorus and nitrogen in a microwave environment. APP is a microwave absorbent salt which served as the dopant source for phosphorus and nitrogen. Synthesis of carbonized materials is illustrated in Scheme 1. Materials were synthesized by addition of 1 g soy precursor (S1—soymeal, S2—hexane processed soymeal, S3—defatted soy flour, S4—soy protein isolate) to 0.8 g of APP in a boron nitride crucible. Table 1 outlines the composition of all materials and the product yield. The dry mixture was homogenized with 500 µL of deionized water and placed into a microwaveable furnace. It was placed and heated in a conventional microwave oven (Panasonic) for 30 min at 2.45 GHz and 1250 Watts of power. After cooling at room temperature, the resulting soy-based phosphorus and nitrogen co-doped carbon was shown to be a clumpy, black solid, which was then grinded into a fine powder with a mortar and pestle.



**Scheme 1.** Components and steps taken to synthesize phosphorus and nitrogen co-doped carbon materials.

**Table 1.** Composition of materials S1–S4.

Material	Soy Precursor (SP)	Amount of SP (g)	Amount of APP (g)	Product Yield (mg)
S1	Soymeal	1	0.8	128
S2	Hexane processed soymeal (HPSM)	1	0.8	98
S3	Soy flour	1	0.8	87
S4	Soy protein isolate (profam)	1	0.8	60

## 2.3. Physical Characterization Methods

Scanning electron microscopy (SEM) was conducted with a JEOL 7000 F instrument for topographical observation of samples. S1–S4 were loaded onto separate aluminum mounts with double-sided carbon tape as preparation for SEM imaging. Surface functionalities and composition of soy materials were determined with a Thermo Scientific K-alpha X-ray photoelectron spectrometer (XPS). Survey and narrow-scan analysis for key surface functional elements were analyzed with Avantage software from Thermo Scientific. Raman spectroscopy was performed to measure the disorder of carbon affected by doping. Raman analysis of the powdered samples was conducted at room temperature using a Horiba Jobin Yvon LabRam HR800 with a charge-coupled detector and spectrometer with a grating of 600 Lines mm<sup>-1</sup>, and an excitation of 632 nm from a He–Ne laser at a 10 mW intensity.

#### 2.4. Electrochemical Methods

Electrochemical measurements were conducted by cyclic voltammetry (CV) utilizing an Epsilon potentiostat using a three-electrode system. The working electrode used was a glassy carbon electrode with the drop-casted conductive material (S1–S4 separately). In order to test the material performance, a slurry was made from co-doped soy material (S1–S4) for loading onto the glassy carbon working electrode. First, the co-doped material was suspended in ethanol and forced into homogenization via sonication with carbon black and an adhesive, Nafion, at a 90:5:5 weight ratio. A 20  $\mu\text{L}$  of the slurry was drop-casted onto the glassy carbon electrode and dried for 8 h at ambient conditions. Platinum wire was used as the counter electrode while two different reference electrodes, i.e., Ag/AgCl and Hg/HgO for the acidic and basic electrolyte, respectively, were utilized. CV measurements were performed using aqueous electrolytes of 1 M  $\text{H}_2\text{SO}_4$  and 6 M KOH which underwent  $\text{N}_2$  gas purge to ensure inert conditions prior to testing. The same conditions were applied for the electrochemical experiments on doped materials at 1.0 M of NaCl,  $\text{NaNO}_3$ , KCl and  $\text{KNO}_3$  salt electrolytes. The Hg/HgO reference electrodes were used for NaCl, while for other salt electrolytes, Ag/AgCl was utilized. Cyclic voltammetry was conducted from a potential range of 0–800 mV in acidic and neutral/salt electrolyte whereas an –1000–0 mV potential range was used for basic conditions. Voltammograms were recorded at various scan rates from 5–100 mV/s. Specific capacitance values were calculated using Equations (1) and (2):

$$I_{avg} = |(I_a + I_c)| \div 2 \quad (1)$$

$$C_s = I_{avg} \div (m \times v) \quad (2)$$

where  $I_{avg}$  is the average peak anodic and cathodic current, measured at around 0.4 V for all materials. The peak currents are depicted by symbols  $I_a$  (anodic) and  $I_c$  (cathodic). The symbol ' $m$ ' represents the mass of the working electrode material, whilst ' $v$ ' correlates to scan rate applied (V/s).

### 3. Results

#### 3.1. Physical Characterization

All soy materials S1–S4 were physically and electrochemically characterized thoroughly. Since each material composition and texture is different, doping with APP results in different characteristics of the resultant products S1–S4.

##### 3.1.1. Scanning Electron Microscopy (SEM)

SEM imaging allows for the detailed topographical analysis of the soy-based co-doped materials. Interestingly, all soy materials displayed distinct morphology since their chemical compositions were not same. As shown in Figure 1, S1 tended to have a flaky but rugged surface morphology with wide depths present, indicative of a porous structure. S2 presented with more clumpy, three-dimensional, spaced-out structures. Indications of pores were not as prevalent in the S2 material compared to S1, S3 and S4, even at higher magnifications. Comparatively, S3 was shown to have a more convoluted topographical appearance with surface depths of different size ranges. At higher magnifications, these depths appeared to be very deep. S4 demonstrated a morphology similar to that of a sponge—flat, with a very distinct holey layout. The SEM image depicted a highly porous morphology of S4 material. At higher magnifications, there were small bubble-like structures occupying the walls of S4. These spherical arrangements have been observed in similar composites that are highly oxidized [43,44]. This may contribute greatly to surface area and pseudocapacitance (electrochemical energy storage) of the material.

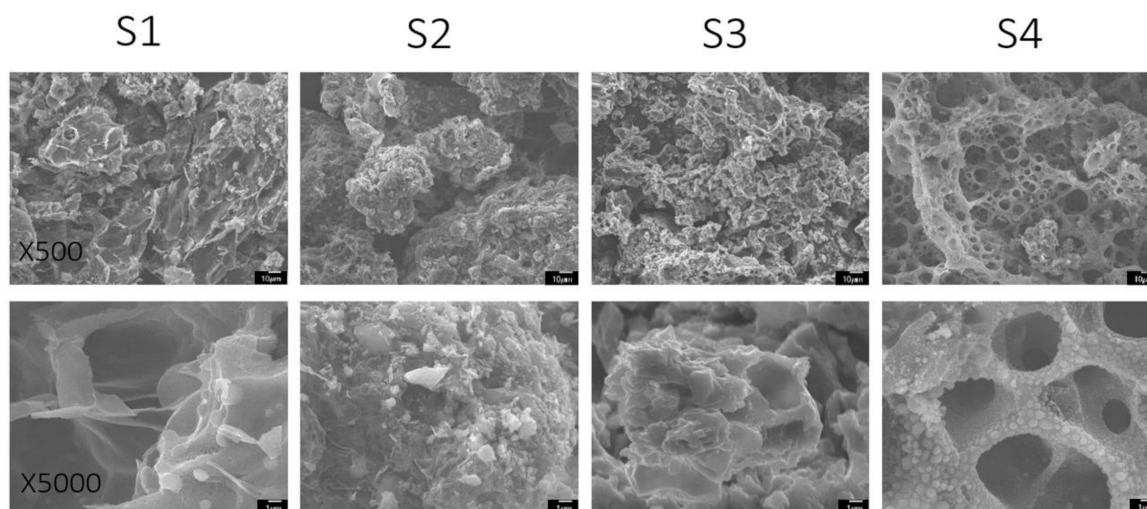


**Figure 1.** SEM images of co-doped soy-based carbon materials at 500× magnification (**top row**) and 5000× magnification (**bottom row**).

### 3.1.2. X-ray Photoelectron Spectroscopy (XPS)

Surface hetero-elemental composition, along with functionality of co-doped soy materials, were explored using XPS, which provides the surface elemental composition and potential functional groups present as deep as 5 nm in the material. Table 2 results show that all materials were significantly composed of carbon with the exception of S3, which was rich in oxygen at the surface. Astonishingly, the very lowest carbon percentage was attained in soy flour after carbonization. The high oxygen element composition at the surface of soy flour is due to the high carbohydrate composition in soybean hulls as well as the preparation of the material's precursor. During the preparation of soy flour, much air is introduced from the sieving process, which can contribute to the high oxygen content in the material. In addition, the presence of hydroxyl groups in the carbohydrates can contribute to form surface oxygen and oxygen functional groups during doping [45,46]. Material S3 is also the least stripped material comparatively, and it demonstrated the highest amounts of phosphorus and potassium—as expected, due to whole soybeans having a naturally rich composition of these two elements. However, the low carbon content of S3 as compared to oxygen may not classify the material as a doped carbon material. All other materials exhibited a significantly high amount of carbon in the carbonized co-doped materials. Moreover, other heteroelements were found in the rest of the materials (S1, S2 and S4) at low concentrations, with a significant decrease in oxygen. In addition, S1 and S2 appeared to have very similar composition. This could be attributed to the fact that the precursors for these two materials are processed in a similar manner. Both soy precursors are of soymeal, which is derived from soybean after the removal of oil and fat. S2 is soymeal further processed with hexane to remove the remaining fats and oils. Whether or not hexane-processing has any significant electrochemical effects, can be determined by investigation of surface functionality of the two materials. S4 contains the highest percentage of carbon at the surface—which is expected, since protein isolate is largely composed of carbons, as well as some additional elements such as nitrogen and oxygen.

Table 3 highlights the surface functional groups that are formed as a result of co-doping and microwave irradiation. As supported by survey scan results, materials S1 and S2 were similar in surface elemental composition; therefore, detailed examination was performed to investigate similarities in the functional groups at the surface of the materials by narrow-scan analysis. However, the two materials displayed slight differences in surface functionality, though the two are very similar compared to that of S3 and S4. The pyridinic and nitrogen oxide functionalities were not observed in S1. Similarly, some functionalities were not present in S2 while S1 possessed them. The most functionalized material seemed

to be S3, in which there was 38% oxygenated carbonyl groups present on the material's surface, supported by a binding energy (BE) value of 533 eV. Oxygen groups tend to play a significant role in electrochemical energy storage [47,48]; however, due to a lower carbon content, one can expect that the S3 material would not show as advantageous a capacitive behavior as S1, S2 and S4. A dramatic decrease in the content of carbon at the surface does not classify S3 as a doped carbon material. All soy materials demonstrated evidence of successful co-doping, as there were topographical functional groups present from phosphorus at BE values of 133–134 eV and nitrogen at a BE of 398–399 eV. These surface functional groups have various conformations due to different reactions with surface carbon. Narrow-scan figures are displayed in Figure S1 of the Supporting Information. Some additional elements such as Mg, Si, and Al were present due to impurities, which contribute to the total atomic percentages present on material surfaces.

**Table 2.** Survey scan results of C1s, N1s, P2p, K2p and O1s core level XPS spectra of soy materials.

Sample	C1s (At%)	N1s (At%)	P2p (At%)	K2p (At%)	O1s (At%)
S1	66.01	1.69	4.11	1.11	27.08
S2	69.65	3.10	6.16	1.03	18.43
S3	18.36	4.17	15.95	2.78	57.30
S4	74.11	0.92	2.12	0.13	22.72

**Table 3.** Detailed narrow scan XPS analysis of functionalities on S1–S4 surfaces. (At%).

Element: Functionality	S1	S2	S3	S4
O1: Quinone	10.12 (531.75 eV)	9.56 (531.64 eV)	17.87 (531.55 eV)	13.35 (531.95 eV)
O2: Carbonyl	16.03 (533.27 eV)	12.04 (533.24 eV)	38.67 (533.07 eV)	9.37 (533.32 eV)
O3: Ether	0.93 (536.19 eV)	~	~	~
P1: Phosphonyl	4.11 (134.22 eV)	6.16 (134.14 eV)	15.95 (134.19 eV)	2.12 (133.81 eV)
P2: P-oxide	0.89 (401.16 eV)	~	~	0.42 (401.53 eV)
N1: Graphitic	0.80 (398.99 eV)	1.20 (398.77 eV)	~	~
N2: Pyridinic	~	0.54 (404.30 eV)	2.28 (401.86 eV)	~
N3: N-oxide	~	2.07 (400.96 eV)	1.52 (399.20 eV)	0.50 (399.07 eV)

### 3.1.3. Raman Spectroscopy

Raman spectroscopy allows an insight into the carbon bonding environment. The spectra displayed two distinct Raman peaks (Figure 2) at Raman shift values of 1350 and 1600  $\text{cm}^{-1}$  for D (defect) and G (graphitic) peaks, respectively, which are characteristic of heterogeneous carbonaceous materials. The D peak, also called the disorder peak, is indicative of  $\text{sp}^2$  carbon functionalization due to doping [49,50]; this mode is not present in perfectly ordered graphite. The G peak, also called the graphitic band, is representative of  $\text{sp}^2$  carbon pair stretching modes. Carbon doping and activation affects surface carbon proportion due to the formation of functional groups via interaction of surface carbon with doping elements and gases formed in the high temperature environment, which causes carbon bond cleavage and formation with reacting species [51,52]. The defect ratio between the integration of these two peaks,  $I_D/I_G$ , gives information related to the degree of doping for the sample.

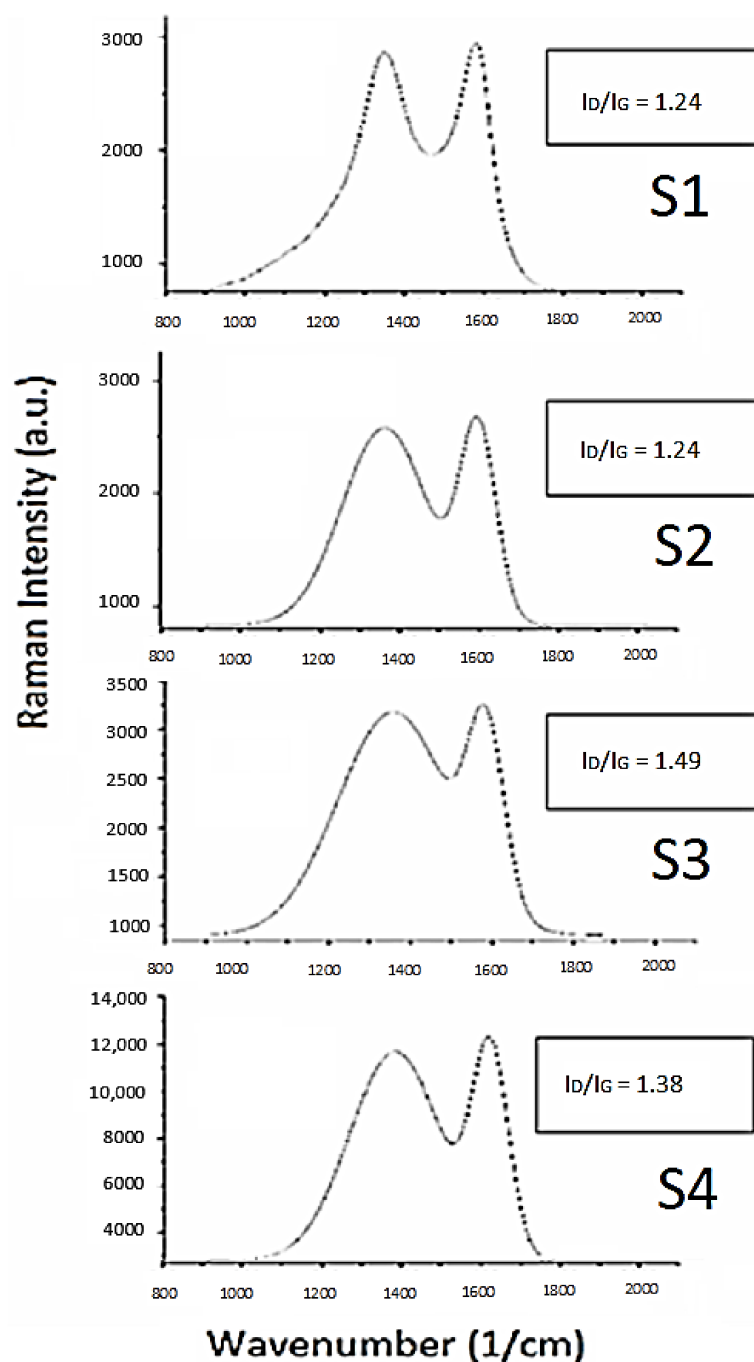


Figure 2. Raman spectra for soy materials.

As shown in Figure 2, all soy materials showed features of functionalized carbon due to phosphorus and nitrogen doping, which is supported by defect ratios above one. S1 exhibits the narrowest D peak, indicative of a smaller amount of doping, whereas the other doped soy materials depict wider D peaks, supporting the higher doping effects of these materials. Material S3 demonstrated the highest amount of disorder, whereas S1 and S2 showed the lowest disorder—which could be due to the soy precursors' reaction pathways during the doping process [53], or simply the presence of a slightly higher degree of graphitization than S3 and S4 [54,55].

### 3.2. Electrochemical Analysis

Cyclic voltammetry was performed to investigate the energy storage potential of the doped carbon materials derived from soy. Electrochemical investigations were conducted

on co-doped soy-based materials S1–S4 in acidic, basic and salt electrolytes. All electrochemical results were analyzed and compared to investigate the potential of soy materials for supercapacitor application. All materials exhibited quasi-rectangular voltammograms, supportive of electric double-layer capacitance (EDLC) as the dominant form of energy storage in the given conditions. As per Figure 3, S1 exhibited the highest current density with a maximum observed specific capacitance of 127 F/g in acidic conditions, as shown in Table 4. The second highest current density was observed for material S4 in acidic conditions with a specific capacitance of 112 F/g. However, the materials did not exhibit a superior performance in basic media. In basic conditions, material S4 had the highest specific capacitance value of 94 F/g. Material S4 seemed to have strong hybrid capacitive behavior compared to the other materials in acidic and basic conditions, given that its specific capacitance values were over 90 F/g in both acidic and basic electrolyte. S4, along with S1 appeared to have better electrochemical performance in  $\text{H}_2\text{SO}_4$ , with a notable decrease in specific capacitance in KOH. S2 electrochemical behavior is very weak; this is attributed to its hexane treatment, which affects its charge storage characteristics. S3 demonstrated the second highest capacitive behavior in basic conditions. Most likely, this is due to the highly oxidized surface shown in Table 2. However, its specific capacitance dropped significantly with increases in scan rates (Figure S2 in the Supplementary Materials). Thus, S3 is a highly unstable material, whereas Figure S2 shows that S1, S2 and S4 sustained 80% specific capacitance when scan rates were altered from 5–100 mV/s. Multiple cycles showed that S3 was the most unstable material among all soy samples.

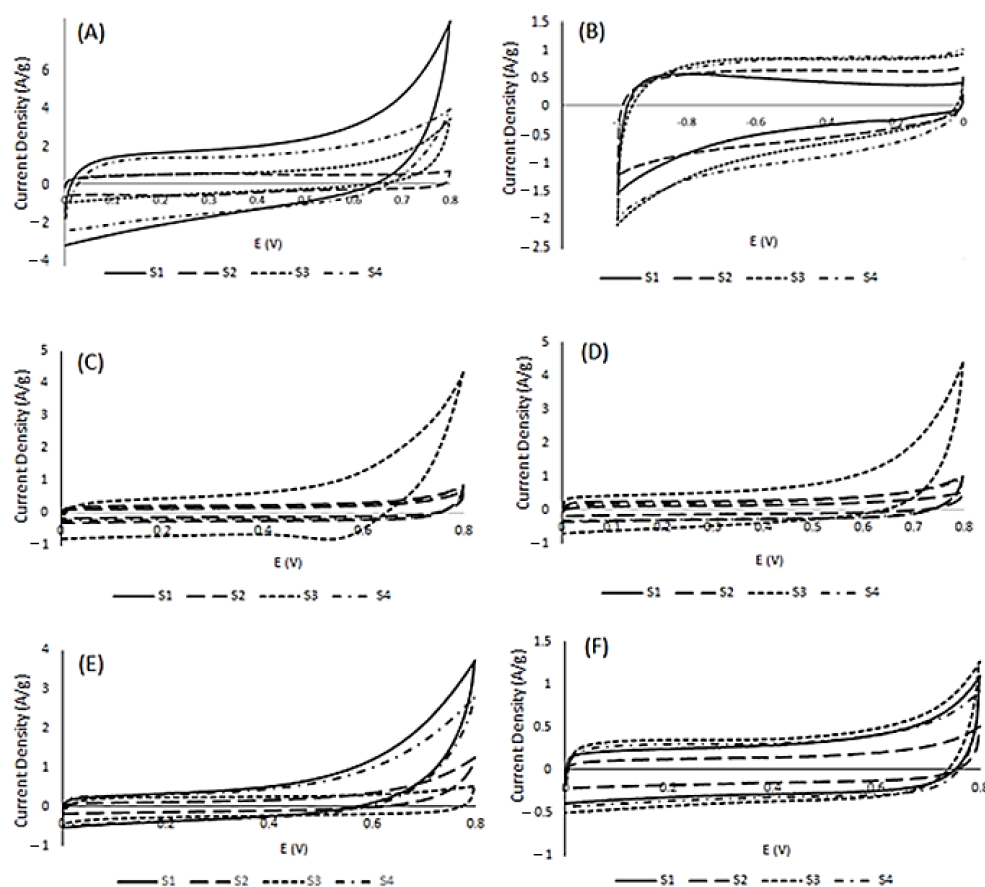


**Figure 3.** Cyclic voltammograms for S1–S4 in acidic (A), basic (B) and salt (KCl (C),  $\text{KNO}_3$  (D),  $\text{NaNO}_3$  (E) and NaCl (F) electrolyte at 10 mV/s.

**Table 4.** Specific capacitance values (F/g) achieved for all soy-based carbon materials in 1 M H<sub>2</sub>SO<sub>4</sub> and 6 M KOH.

Material	SC <sub>H<sub>2</sub>SO<sub>4</sub></sub>	SC <sub>KOH</sub>	SC <sub>KCl</sub>	SC <sub>KNO<sub>3</sub></sub>	SC <sub>NaCl</sub>	SC <sub>NaNO<sub>3</sub></sub>
S1	127	47	25	31	30	103
S2	56	68	15	16	15	17
S3	77	91	87	74	40	36
S4	112	94	21	27	32	67

In an effort to further explore the electrochemical behavior of soy-based doped carbons, CVs were conducted using S1–S4 in salt electrolytes. Salt electrolytes are cost-efficient and environmentally safe and stable. Double-layer formation at the surface of electrode with the electrolyte is an important aspect of electrochemical energy storage; thus, an exploratory approach was taken to investigate the role of ionic size. In this regard, four salts: NaNO<sub>3</sub>, NaCl, KNO<sub>3</sub> and KCl, were selected to investigate the effect of cation and anion size on electrochemical performance. Sodium is smaller in size compared to potassium, whereas chloride is smaller than nitrate. As per Figure 3, there is a significant difference in the interactions between the co-doped materials with salt electrolytes. Compared to the soy materials' behavior in acidic and basic conditions, S3 exhibited the most prevalent voltammogram, with a reduction peak shown at around 0.55 V potential in KCl—indicative of oxygen reduction, a form of pseudocapacitance. This is presumably due to differences in ion diffusion, which in turn affects current density and subsequently the specific capacitance. The second highest specific capacitance achieved in salt electrolytes was from S1, with a specific capacitance value of 103 F/g in NaCl. S1 exhibited a higher ionic compatibility than materials S2–S4 with the sodium salts. All materials except S3 exhibited a superior supercapacitance value in the presence of nitrate anions as compared to chloride anions. A superior electrochemical behavior was observed in the presence of sodium cations in comparison to potassium ions. The superior performance of sodium cations can be attributed to the penetration of small cations on the pores at the surface of the soy electrode materials. However, an opposite behavior was observed in the case of the anion. Chloride is smaller than nitrate, but the EDLC performance of nitrate ion is better due to the presence of functional groups at the surface of S1–S4 materials, which interact better with nitrate. Thus, NaNO<sub>3</sub> is the best electrolyte for soy-based doped carbon electrodes.

Previously, soy materials have been explored for supercapacitor applications. For example, pyrolyzed soybean hulls were used for the synthesis of KOH-activated carbons (AC) by Herde et al. [32]. They performed electrochemical measurements in tetraethylammonium hexafluorophosphate, with propylene carbonate as the electrolyte. Another report from Huo et al. [31], used soy protein isolate as the base of an ethylene glycol diglycidyl ether (EGDE)-crosslinked hydrogel for implementation as a solid-state supercapacitor electrolyte. The soy-based supercapacitor systems employed by Herde et al. and Huo et al. displayed sufficient electrochemical behavior with specific capacitance values ranging from 4–115 F/g. In this work, the highest specific capacitance value obtained was 127 F/g in acidic conditions for soy material, in comparison to previously published studies. Moreover, a simple microwave-assisted synthesis of carbonized materials from soy product resulted in a very high specific capacitance of 103 F/g in aqueous salt electrolyte.

#### 4. Conclusions

Here, co-doped carbons were synthesized using four different soy products. All materials demonstrated successful doping of phosphorus or nitrogen with an ammonium polyphosphate doping agent. In addition, oxygen functional groups were the most prevalent in all materials. These materials were physically characterized in detail. Their surface morphology and surface elemental composition, along with their functional groups and carbon-bonding environment were evaluated using SEM, XPS and Raman spectroscopy,

respectively. These materials are also used as active materials at the surface of a working electrode in cyclic voltammetry experiments. The charge storage capabilities of all four materials were investigated at different scan rates in acidic and basic, as well as salt, electrolytes. Four different salts were used to investigate the role of cations and anions on supercapacitor performance. The greatest value of specific capacitance achieved for all materials was 127 F/g in acidic conditions. The greatest value achieved in basic conditions was 94 F/g. All of the parameters discussed, such as surface functionality and topographical morphology, play a role in electrochemical behavior and energy storage in acidic, basic and neutral salt conditions. The optimal material in most commonly used aqueous electrolytes was deemed to be S4, due to its comparatively exemplary features, such as its highly functionalized surface and high energy storage values in both acidic and basic conditions that are ideal for a supercapacitor material. Material S3 was shown to be better in neutral conditions, which are essentially greener and more cost-efficient compared to the commonly utilized acidic and basic aqueous conditions for electrochemical applications of conductive, carbon-based materials, but it is highly unstable due to its higher oxygen contents. The sodium cation and nitrate anion showed better performances compared to potassium and chloride. Thus, the charge storage performance of these materials can be further improved by changing the doping agent concentration, as well as using different ionic sizes in salt electrolyte, which can affect surface morphology, functionalities and electrochemical behavior in aqueous electrolytes.

**Supplementary Materials:** The following are available online at <https://www.mdpi.com/article/10.3390/electrochem2040034/s1>, Figure S1: Narrow scan compilation of soy-based PNDC materials. Figure S2: Plot of specific capacitance with relation to scan rate in KCl (left) and KNO<sub>3</sub> (right).

**Author Contributions:** Conceptualization, I.D. and A.K.; methodology, I.D.; software, F.W.; validation, I.D.; formal analysis, A.K. and I.D.; investigation, I.D., N.S.; resources, T.V.; data curation, I.D., A.K. and T.S.; writing—original draft preparation, I.D. and A.K.; writing—review and editing, N.S.; visualization, I.D.; supervision, N.S.; project administration, N.S.; funding acquisition, N.S. and I.D. All authors have read and agreed to the published version of the manuscript.

**Funding:** This research acknowledges the Signature award funding and startup funds from the University of Arkansas at Little Rock.

**Institutional Review Board Statement:** Not applicable.

**Informed Consent Statement:** Not applicable.

**Data Availability Statement:** Data available in a publicly accessible repository.

**Acknowledgments:** We thank Shawn Bourdo and Ahmad Alam for their help.

**Conflicts of Interest:** The authors declare no conflict of interest.

## References

1. Barreto, R.A. Fossil fuels, alternative energy and economic growth. *Econ. Model.* **2018**, *75*, 196–220. [[CrossRef](#)]
2. Behrens, A.; Giljum, S.; Kovanda, J.; Niza, S. The material basis of the global economy: Worldwide patterns of natural resource extraction and their implications for sustainable resource use policies. *Ecol. Econ.* **2007**, *64*, 444–453. [[CrossRef](#)]
3. Palmer, G. Renewables rise above fossil fuels. *Nat. Energy* **2019**, *4*, 538–539. [[CrossRef](#)]
4. Afif, A.; Rahman, S.M.; Azad, A.T.; Zaini, J.; Islam, A.; Azad, A. Advanced materials and technologies for hybrid supercapacitors for energy storage—A review. *J. Energy Storage* **2019**, *25*, 100852. [[CrossRef](#)]
5. Sharma, P.; Kumar, V. Current Technology of Supercapacitors: A Review. *J. Electron. Mater.* **2020**, *49*, 3520–3532. [[CrossRef](#)]
6. Farcas, C.; Petreus, D.; Ciocan, I.; Palaghita, N. Modeling and simulation of supercapacitors. In Proceedings of the 2009 15th International Symposium for Design and Technology of Electronics Packages (SIITME), Gyula, Hungary, 17–20 September 2009; pp. 195–200. [[CrossRef](#)]
7. Liu, P.; Verbrugge, M.; Soukiazian, S. Influence of temperature and electrolyte on the performance of activated-carbon supercapacitors. *J. Power Sources* **2006**, *156*, 712–718. [[CrossRef](#)]
8. Muzaffar, A.; Ahamed, M.B.; Deshmukh, K.; Thirumalai, J. A review on recent advances in hybrid supercapacitors: Design, fabrication and applications. *Renew. Sustain. Energy Rev.* **2018**, *101*, 123–145. [[CrossRef](#)]

9. Kolur, N.A.; Sharifian, S.; Kaghazchi, T. Investigation of sulfuric acid-treated activated carbon properties. *Turk. J. Chem.* **2019**, *43*, 663–675. [CrossRef]
10. Nguyen, T.; Montemor, M.D.F. Metal Oxide and Hydroxide-Based Aqueous Supercapacitors: From Charge Storage Mechanisms and Functional Electrode Engineering to Need-Tailored Devices. *Adv. Sci.* **2019**, *6*, 1801797. [CrossRef]
11. Hassan, I.U.; Salim, H.; Naikoo, G.A.; Awan, T.; Dar, R.A.; Arshad, F.; Tabidi, M.A.; Das, R.; Ahmed, W.; Asiri, A.M.; et al. A review on recent advances in hierarchically porous metal and metal oxide nanostructures as electrode materials for supercapacitors and non-enzymatic glucose sensors. *J. Saudi Chem. Soc.* **2021**, *25*, 101228. [CrossRef]
12. Ghosh, S.; Santhosh, R.; Jeniffer, S.; Raghavan, V.; Jacob, G.; Nanaji, K.; Kollu, P.; Jeong, S.K.; Grace, A.N. Natural biomass derived hard carbon and activated carbons as electrochemical supercapacitor electrodes. *Sci. Rep.* **2019**, *9*, 1–15. [CrossRef]
13. Liang, R.; Du, Y.; Xiao, P.; Cheng, J.; Yuan, S.; Chen, Y.; Yuan, J.; Chen, J. Transition Metal Oxide Electrode Materials for Supercapacitors: A Review of Recent Developments. *Nanomaterials* **2021**, *11*, 1248. [CrossRef]
14. Abioye, A.M.; Ani, F.N. Recent development in the production of activated carbon electrodes from agricultural waste biomass for supercapacitors: A review. *Renew. Sustain. Energy Rev.* **2015**, *52*, 1282–1293. [CrossRef]
15. Zhang, J.; Jin, L.; Cheng, J.; Hu, H. Hierarchical porous carbons prepared from direct coal liquefaction residue and coal for supercapacitor electrodes. *Carbon* **2012**, *55*, 221–232. [CrossRef]
16. Ramasahayam, S.K.; Hicks, Z.; Viswanathan, T. Thiamine-Based Nitrogen, Phosphorus, and Silicon Tri-doped Carbon for Supercapacitor Applications. *ACS Sustain. Chem. Eng.* **2015**, *3*, 2194–2202. [CrossRef]
17. Castro-Gutiérrez, J.; Díez, N.; Sevilla, M.; Izquierdo, M.T.; Ghanbaja, J.; Celzard, A.; Fierro, V. High-Rate Capability of Supercapacitors Based on Tannin-Derived Ordered Mesoporous Carbons. *ACS Sustain. Chem. Eng.* **2019**, *7*, 17627–17635. [CrossRef]
18. Ramasahayam, S.K.; Nasini, U.B.; Shaikh, A.U.; Viswanathan, T. Novel tannin-based Si, P co-doped carbon for supercapacitor applications. *J. Power Sources* **2015**, *275*, 835–844. [CrossRef]
19. Macchi, S.; Siraj, N.; Watanabe, F.; Viswanathan, T. Renewable Tannin-Based Dual-Doped Carbon Material and its Application as a Supercapacitor Electrode Material. *Curr. Res. Mater. Chem.* **2019**, *1*, 101.
20. Song, X.; Ma, X.; Li, Y.; Ding, L.; Jiang, R. Tea waste derived microporous active carbon with enhanced double-layer supercapacitor behaviors. *Appl. Surf. Sci.* **2019**, *487*, 189–197. [CrossRef]
21. Inal, I.I.G.; Holmes, S.; Banford, A.; Aktas, Z. The performance of supercapacitor electrodes developed from chemically activated carbon produced from waste tea. *Appl. Surf. Sci.* **2015**, *357*, 696–703. [CrossRef]
22. Adan-Mas, A.; Alcaraz, L.; Arévalo-Cid, P.; López-Gómez, F.A.; Montemor, F. Coffee-derived activated carbon from second biowaste for supercapacitor applications. *Waste Manag.* **2020**, *120*, 280–289. [CrossRef]
23. Rufford, T.; Hulicova-Jurcakova, D.; Zhu, Z.; Lu, G. Nanoporous carbon electrode from waste coffee beans for high performance supercapacitors. *Electrochem. Commun.* **2008**, *10*, 1594–1597. [CrossRef]
24. Yun, Y.S.; Park, M.H.; Hong, P.M.; Lee, M.E.; Park, Y.W.; Jin, H.-J. Hierarchically Porous Carbon Nanosheets from Waste Coffee Grounds for Supercapacitors. *ACS Appl. Mater. Interfaces* **2015**, *7*, 3684–3690. [CrossRef]
25. Xi, Y.; Cao, J.; Li, J.; Zhang, P.; Zhu, Y.; Han, W. High-rate supercapacitor based on 3D hierarchical N-doped porous carbon derived from sustainable spongy cornstalk pith. *J. Energy Storage* **2021**, *37*, 102470. [CrossRef]
26. Wang, L.; Mu, G.; Tian, C.; Sun, L.; Zhou, W.; Yu, P.; Yin, J.; Fu, H. Porous Graphitic Carbon Nanosheets Derived from Cornstalk Biomass for Advanced Supercapacitors. *ChemSusChem* **2013**, *6*, 880–889. [CrossRef]
27. Denmark, I.; Macchi, S.; Watanabe, F.; Viswanathan, T.; Siraj, N. Effect of KOH on the Energy Storage Performance of Molasses-Based Phosphorus and Nitrogen Co-Doped Carbon. *Electrochem* **2021**, *2*, 3. [CrossRef]
28. Kiełbasa, K.; Adrianna, K.; Nikola, M. Studies of the preparation of the microporous carbon materials from molasses. In *The Book of Articles National Scientific Conference “e-Factory of Science”*; Medical University of Lodz: Lodz, Poland, 2020; pp. 27–73.
29. Yu, J.; Li, M.; Wang, X.; Yang, Z. Promising High-Performance Supercapacitor Electrode Materials from MnO<sub>2</sub> Nanosheets@Bamboo Leaf Carbon. *ACS Omega* **2020**, *5*, 16299–16306. [CrossRef]
30. Bazan-Aguilar, A.; Ponce-Vargas, M.; Caycho, C.L.; La Rosa-Toro, A.; Baena-Moncada, A.M. Highly Porous Reduced Graphene Oxide-Coated Carbonized Cotton Fibers as Supercapacitor Electrodes. *ACS Omega* **2020**, *5*, 32149–32159. [CrossRef]
31. Huo, P.; Ni, S.; Hou, P.; Xun, Z.; Liu, Y.; Gu, J. A Crosslinked Soybean Protein Isolate Gel Polymer Electrolyte Based on Neutral Aqueous Electrolyte for a High-Energy-Density Supercapacitor. *Polymers* **2019**, *11*, 863. [CrossRef]
32. Herde, Z.; Dharmasena, R.; Sumanasekera, G.; Tumuluru, J.S.; Satyavolu, J. Impact of hydrolysis on surface area and energy storage applications of activated carbons produced from corn fiber and soy hulls. *Carbon Resour. Convers.* **2019**, *3*, 19–28. [CrossRef]
33. Ross, J. Arkansas Soybean Research Studies 2019; 2020. Available online: <https://scholarworks.uark.edu/aeesser/166/> (accessed on 18 August 2021).
34. Peng, S.; Cho, K. Ab Initio Study of Doped Carbon Nanotube Sensors. *Nano Lett.* **2003**, *3*, 513–517. [CrossRef]
35. Konar, S.; Kumar, B.P.; Mahto, M.K.; Samanta, D.; Shaik, A.S.; Shaw, M.; Mandal, M.; Pathak, A. N-doped carbon dot as fluorescent probe for detection of cysteamine and multicolor cell imaging. *Sens. Actuators B Chem.* **2019**, *286*, 77–85. [CrossRef]
36. Kim, M.-J.; Park, J.E.; Kim, S.; Lim, M.S.; Jin, A.; Kim, O.-H.; Kim, M.J.; Lee, K.-S.; Kim, J.; Kim, S.-S.; et al. Biomass-Derived Air Cathode Materials: Pore-Controlled S,N-Co-doped Carbon for Fuel Cells and Metal–Air Batteries. *ACS Catal.* **2019**, *9*, 3389–3398. [CrossRef]

37. Macchi, S.; Siraj, N.; Watanabe, F.; Viswanathan, T. Renewable-Resource-Based Waste Materials for Supercapacitor Application. *ChemistrySelect* **2019**, *4*, 492–501. [[CrossRef](#)]
38. Miao, L.; Duan, H.; Wang, Z.; Lv, Y.; Xiong, W.; Zhu, D.; Gan, L.; Li, L.; Liu, M. Improving the pore-ion size compatibility between poly(ionic liquid)-derived carbons and high-voltage electrolytes for high energy-power supercapacitors. *Chem. Eng. J.* **2020**, *382*, 122945. [[CrossRef](#)]
39. Masarapu, C.; Wang, L.-P.; Li, X.; Wei, B. Tailoring Electrode/Electrolyte Interfacial Properties in Flexible Supercapacitors by Applying Pressure. *Adv. Energy Mater.* **2012**, *2*, 546–552. [[CrossRef](#)]
40. Pal, B.; Yang, S.; Ramesh, S.; Thangadurai, V.; Jose, R. Electrolyte selection for supercapacitive devices: A critical review. *Nanoscale Adv.* **2019**, *1*, 3807–3835. [[CrossRef](#)]
41. Zhao, N.; Fan, H.; Zhang, M.; Ma, J.; Zhang, W.; Wang, C.; Li, H.; Jiang, X.; Cao, X. Investigating the large potential window of NiCo<sub>2</sub>O<sub>4</sub> supercapacitors in neutral aqueous electrolyte. *Electrochim. Acta* **2019**, *321*. [[CrossRef](#)]
42. Li, J.; An, L.; Li, H.; Sun, J.; Shuck, C.; Wang, X.; Shao, Y.; Li, Y.; Zhang, Q.; Wang, H. Tunable stable operating potential window for high-voltage aqueous supercapacitors. *Nano Energy* **2019**, *63*, 103848. [[CrossRef](#)]
43. Tran, H.N.; Huang, F.-C.; Lee, C.-K.; Chao, H.-P. Activated carbon derived from spherical hydrochar functionalized with triethylenetetramine: Synthesis, characterizations, and adsorption application. *Green Process. Synth.* **2017**, *6*, 565–576. [[CrossRef](#)]
44. Tripathi, N.K. Porous carbon spheres: Recent developments and applications. *AIMS Mater. Sci.* **2018**, *5*, 1016–1052. [[CrossRef](#)]
45. Chen, N.; Zeng, Q.; Lin, Q.; Rao, J. Development of defatted soy flour based bio-adhesives using *Viscozyme L*. *Ind. Crop. Prod.* **2015**, *76*, 198–203. [[CrossRef](#)]
46. Plonska-Brzezinska, M.E.; Molina-Ontoria, A.; Echegoyen, L. Post-modification by low-temperature annealing of carbon nanoions in the presence of carbohydrates. *Carbon* **2014**, *67*, 304–317. [[CrossRef](#)]
47. Cao, H.; Peng, X.; Zhao, M.; Liu, P.; Xu, B.; Guo, J. Oxygen functional groups improve the energy storage performances of graphene electrochemical supercapacitors. *RSC Adv.* **2018**, *8*, 2858–2865. [[CrossRef](#)]
48. Chen, Y.; Zhang, Z.; Huang, Z.; Zhang, H. Effects of oxygen-containing functional groups on the supercapacitor performance of incompletely reduced graphene oxides. *Int. J. Hydrogen Energy* **2016**, *42*, 7186–7194. [[CrossRef](#)]
49. Hu, H.; Bin Zhao, B.; Hamon, M.A.; Kamaras, K.; Itkis, A.M.E.; Haddon, R.C. Sidewall Functionalization of Single-Walled Carbon Nanotubes by Addition of Dichlorocarbene. *J. Am. Chem. Soc.* **2003**, *125*, 14893–14900. [[CrossRef](#)]
50. Curran, S.A.; Ellis, A.; Vijayaraghavan, A.; Ajayan, P.M. Functionalization of carbon nanotubes using phenosafranin. *J. Chem. Phys.* **2004**, *120*, 4886. [[CrossRef](#)]
51. Manioudakis, J.; Victoria, F.; Thompson, C.A.; Brown, L.; Movsum, M.; Lucifero, R.; Naccache, R. Effects of nitrogen-doping on the photophysical properties of carbon dots. *J. Mater. Chem. C* **2018**, *7*, 853–862. [[CrossRef](#)]
52. Gao, Y.; Wang, Q.; Ji, G.; Li, A.; Niu, J. Doping strategy, properties and application of heteroatom-doped ordered mesoporous carbon. *RSC Adv.* **2021**, *11*, 5361–5383. [[CrossRef](#)]
53. Guizani, C.; Haddad, K.; Limousy, L.; Jeguirim, M. New insights on the structural evolution of biomass char upon pyrolysis as revealed by the Raman spectroscopy and elemental analysis. *Carbon* **2017**, *119*, 519–521. [[CrossRef](#)]
54. Wu, Q.; Gao, J.; Feng, J.; Liu, Q.; Zhou, Y.; Zhang, S.; Nie, M.; Liu, Y.; Zhao, J.; Liu, F.; et al. A CO<sub>2</sub> adsorption dominated carbon defect-based electrocatalyst for efficient carbon dioxide reduction. *J. Mater. Chem. A* **2019**, *8*, 1205–1211. [[CrossRef](#)]
55. Choudhary, H.K.; Kumar, R.; Pawar, S.P.; Sundararaj, U.; Sahoo, B. Enhancing absorption dominated microwave shielding in Co@C–PVDF nanocomposites through improved magnetization and graphitization of the Co@C-nanoparticles. *Phys. Chem. Chem. Phys.* **2019**, *21*, 15595–15608. [[CrossRef](#)]